Rap1 controls cell adhesion and cell motility through the regulation of myosin II

Taeck J. Jeon,[1] Dai-Jen Lee,[1] Sylvain Merlot,[1] Gerald Weeks,[2] and Richard A. Firtel[1]

[1]Section of Cell and Developmental Biology, Division of Biological Sciences, Center for Molecular Genetics, University of California, San Diego, La Jolla, CA 92093
[2]Department of Microbiology and Immunology, University of British Columbia, Vancouver, British Columbia V6T 1Z3, Canada

We have investigated the role of Rap1 in controlling chemotaxis and cell adhesion in *Dictyostelium discoideum*. Rap1 is activated rapidly in response to chemoattractant stimulation, and activated Rap1 is preferentially found at the leading edge of chemotaxing cells. Cells expressing constitutively active Rap1 are highly adhesive and exhibit strong chemotaxis defects, which are partially caused by an inability to spatially and temporally regulate myosin assembly and disassembly. We demonstrate that the kinase Phg2, a putative Rap1 effector, colocalizes with Rap1–guanosine triphosphate at the leading edge and is required in an in vitro assay for myosin II phosphorylation, which disassembles myosin II and facilitates filamentous actin–mediated leading edge protrusion. We suggest that Rap1/Phg2 plays a role in controlling leading edge myosin II disassembly while passively allowing myosin II assembly along the lateral sides and posterior of the cell.

Introduction

Rap1 has been implicated in the control of cell adhesion in a variety of cell types (Stork, 2003; Bos, 2005; Kinashi and Katagiri, 2005; Retta et al., 2006). In mammalian cells, Rap1 controls cell spreading by mediating the functions of integrins, by binding to and localizing the Rac exchange factors (guanine nucleotide exchange factors [GEFs]) VAV1 and TIAM1 to the sites of cell spreading, and by regulating cadherin-mediated cell–cell contacts (Bos et al., 2003; Arthur et al., 2004; Enserink et al., 2004; Fukuyama et al., 2005; Kinashi and Katagiri, 2005; Fukuhra et al., 2006). Rap1 is thought to control cell adhesion and the leading edge function of moving cells by interacting with and regulating adaptor proteins that help control the cytoskeleton, although there is no direct evidence of a regulatory role for Rap1. RIAM and lamellipodin are related members of the MRL family of adaptor proteins containing a Ras association (RA) Rap1-GTP–binding domain, a PI(3,4)P_2-binding pleckstrin homology (PH) domain, and a polyproline domain that interacts with Ena–vasodilator-stimulated phosphoprotein and profilin. RIAM1 induces cell spreading and lamellipodia formation and localizes to the sites of membrane protrusion (Lafuente et al., 2004), whereas lamellipodin controls leading edge formation and filamentous actin (F-actin) polymerization in PDGF-treated fibroblasts (Krause et al., 2004). Other Rap1 effectors include the following: affidin, which is associated with cell junctions and binds ZO-1, nectins, and profilin and, thus, may provide a link between Rap1 and the regulation of F-actin filaments (Asakura et al., 1999); RapL, which binds LFA-1 (lymphocyte function–associated antigen 1) and regulates LFA-1 localization in a Rap1-GTP–dependent manner (Fujita et al., 2005); ARAP3, which contains an Arf6 GTPase-activating protein, a RhoA GTPase-activating protein domain, and several PH domains and affects PDGF-induced lamellipodia formation (Krugmann et al., 2006); and PDZ-GEF, a Rap1-GTP–binding Rap1-GEF (Rebhun et al., 2000; Lee et al., 2002).

In *Dictyostelium discoideum*, Rap1 has been linked to cytoskeletal regulation, phagocytosis, and the response to osmotic stress (Rebstein et al., 1993, 1997; Kang et al., 2002). The overexpression of wild-type Rap1 leads to cell spreading and reduces the contraction of cells in response to treatment with azide. The reduction of Rap1 expression suppresses osmotic stress–induced cyclic guanosine monophosphate (cGMP) production and impairs cell viability, whereas the expression of constitutively active $Rap1^{G12V}$ enhances cGMP production (Kang et al., 2002). Osmotic stress causes the activation of Rap1 with kinetics paralleling those of cGMP production. Rap1 was implicated in phagocytosis by an analysis of the putative Rap1 effector Phg2, a kinase with an RA domain that preferentially

Correspondence to Richard A. Firtel: rafirtel@ucsd.edu

S. Merlot's present address is Institut des Sciences du Végétal, Centre National de la Recherche Scientifique, 91190 Gif-sur-Yvette, France.

Abbreviations used in this paper: cGMP, cyclic guanosine monophosphate; F-actin, filamentous actin; GEF, guanine nucleotide exchange factor; MHCK, myosin II heavy chain kinase; PH, pleckstrin homology; RA, Ras association; RBD, Ras-binding domain.

The online version of this article contains supplemental material.

Supplemental material can be found at:
http://doi.org/10.1083/jcb.200607072

The Journal of Cell Biology, Vol. 176, No. 7, March 26, 2007 1021–1033
http://www.jcb.org/cgi/doi/10.1083/jcb.200607072

binds Rap1-GTP but not Ras-GTP (Gebbie et al., 2004). This *phg2*-null strain exhibits defects in particle binding during phagocytosis, cell substratum adhesion, and motility.

The mechanisms by which Rap1 controls cytoskeletal reorganizations in *D. discoideum* are not understood. To investigate this, we analyzed the role of Rap1 in cell adhesion and chemotaxis and found that Rap1 controls myosin II assembly and disassembly. We demonstrate that Rap1 is activated at the cell's cortex and preferentially at the leading edge of chemotaxing cells, the site at which Phg2 localizes. Cells expressing constitutively active Rap1 are unable to effectively regulate myosin II assembly and disassembly. We determined that Phg2 is required for myosin II phosphorylation in an in vitro assay. Our findings suggest a model in which localized recruitment to and activation of Phg2 at the leading edge by Rap1-GTP of chemotaxing cells are required for proper myosin II phosphorylation and disassembly at the newly formed pseudopod. We suggest that this leading edge activation of Rap1 regulates cell adhesion and, during chemotaxis, helps establish cell polarity by locally modulating myosin II assembly and disassembly.

Results

Rap1 is activated in response to chemoattractant stimulation

D. discoideum has a single Ras subfamily member that is homologous to human Rap1 (Weeks et al., 2005). We investigated whether *D. discoideum* Rap1 plays a role in chemotaxis by examining kinetics of the chemoattractant (cAMP)-mediated activation of endogenous Rap1 and myc-tagged wild-type, constitutively active ($Rap1^{G12V}$), and dominant-negative *D. discoideum* Rap1 ($Rap1^{S17N}$) expressed in *D. discoideum* cells. We used a pull-down assay using the human RalGDS Rap1-GTP–binding domain, which shows high but not exclusive specificity for the GTP-bound form of Rap1 and only poorly binds Ras-GTP in crude extracts in this assay (Fig. 1 E; see Materials and methods; Herrmann et al., 1996; Franke et al., 1997). Fig. 1 A shows that endogenous Rap1 was rapidly activated in response to stimulation, with a peak at 5–10 s. Myc-Rap1 ($Rap1^{OE}$) expressed in wild-type cells displayed a similar activation profile (Fig. 1 A). There was a high level of

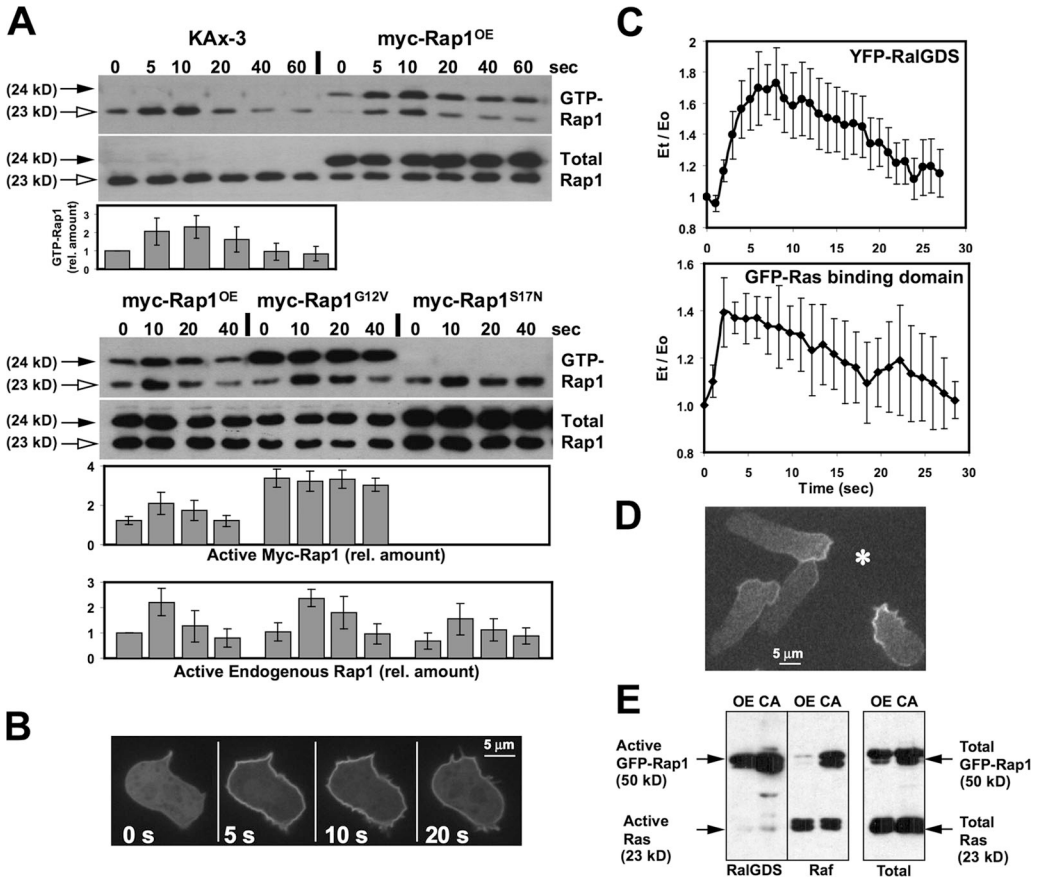

Figure 1. **Activation of Rap1 by cAMP.** (A) The activation level of endogenous Rap1 (open arrow) or myc-Rap1 (closed arrow) in response to cAMP was assayed using a GST-RapBD pull-down assay (see Materials and methods). Wild-type cells or cells expressing myc-Rap1 were stimulated with cAMP for the indicated times and analyzed by immunoblot assay using an antibody against Rap1. The data were quantitated by densitometry and normalized to total Rap1. (B) The translocation of RapBD-RalGDS-YFP to the membrane in response to uniform chemoattractant stimulation was imaged. (C) Translocation kinetics of RapBD-RalGDS-YFP or GFP-RasBD were obtained from time-lapse recordings and quantitated as described previously (Sasaki et al., 2004). The graphs represent the mean of data on several cells from videos taken from at least three separate experiments. Error bars represent SD. (D) Spatial localization of activated Rap1 in migrating cells. The asterisk indicates the position of the micropipette containing cAMP. (E) Lysates from cells expressing GFP fusion wild-type Rap1 (OE) or constitutive Rap1 (CA) were used in the pull-down assay using GST-RalGDS-RBD or GST-Raf1-RBD. The samples were subjected to SDS-PAGE and immunoblotted using an anti-GFP antibody or anti-pan Ras antibody.

myc-Rap1^{G12V} in the GTP-bound form in unstimulated cells, and the level did not change on stimulation. Myc-Rap1^{S17N}, which was expressed at approximately the same level as myc-Rap1^{OE} and myc-Rap1^{G12V}, did not exhibit binding before or after stimulation. The relative (normalized) level of endogenous Rap1-GTP (level of Rap1-GTP compared with total Rap1 as determined by Western blotting) was slightly reduced in cells expressing Rap1^{S17N}.

Spatial localization of activated Rap1

We investigated Rap1 localization using GFP-Rap1 and myc-Rap1. GFP-Rap1 exhibited the same activation kinetics as endogenous Rap1 or myc-Rap1, indicating that it was biologically active (unpublished data). GFP-Rap1 and myc-Rap1 localized predominantly to intracellular membranes, including the ER and endosomal membranes, which is similar to observations in mammalian cells (Fig. 2, A–C; Berger et al., 1994; Ohba et al., 2003; Bivona et al., 2004). In addition, a portion of GFP-Rap1 was present on the plasma membrane. This is more readily seen after removal of the soluble cytoplasmic fraction (Fig. 2 F). Total GFP-Rap1 showed a similar localization in chemotaxing cells and is absent from the domain immediately posterior to the leading edge, presumably because the endosomal membrane fraction is excluded by the pseudopodial F-actin cortex (Fig. 2 E). The localization of total Rap1 is not detectably altered on global (uniform) chemoattractant stimulation (Fig. 2 D). GFP-Rap1^{G12V} exhibited a similar subcellular localization (unpublished data).

We created a YFP-RalGDS reporter to examine the spatial-temporal activation of Rap1 (Bivona et al., 2004). We observed a low level of Rap1-GTP (localized YFP-RapBD) at the plasma membrane before chemoattractant stimulation, which is consistent with a basal level of Rap1-GTP in these cells. In response to chemoattractant stimulation, Rap1-GTP levels at the cell cortex rapidly increase within 3 s of stimulation and peak at ~6–8 s (Fig. 1, B and C). These Rap1 kinetics are slower than those of Ras (Fig. 1 C; Sasaki et al., 2004). In chemotaxing cells, Rap1-GTP is found predominantly at the leading edge and extends weakly along the sides of cells (Fig. 1 D). This domain of Rap1-GTP is broader than that observed for Ras-GTP (Sasaki et al., 2004). No localization of the YFP-RapBD reporter is observed on vesicles and other intracellular membranes where the majority of Rap1 is found, suggesting that Rap1-GTP activation is restricted to the cortex.

Rap1 controls cell adhesion and regulates chemotaxis

Cells overexpressing wild-type Rap1 (Rap1^{OE} cells) are more flattened and spread than wild-type cells as previously described (Fig. 3 A; Rebstein et al., 1993, 1997). This phenotype is substantially enhanced in cells overexpressing Rap1^{G12V} and reduced in cells overexpressing Rap1^{S17N} (Fig. 3 A), suggesting that Rap1 may control cell-substratum attachment. This conclusion was confirmed using cell-substratum attachment assays, which measure the fraction of cells that detach from a membrane during agitation. Rap1-overexpressing cells exhibit a small increase in cell attachment (i.e., a decrease in cell detachment; Fig. 3 B and Fig. S1, available at http://www.jcb.org/cgi/content/full/jcb.200607072/DC1). The level of cell attachment is considerably greater for Rap1^{G12V} cells. We were unable to obtain a Rap1 knockout, suggesting that Rap1 is essential. To examine the phenotype of cells exhibiting reduced Rap1-GTP levels, we expressed Rap1^{S17N} in wild-type cells. Although expressing Rap1^{S17N} has little effect on endogenous Rap1 activation (Fig. 1 A), Rap1^{S17N} cells exhibit reduced attachment.

Unconventional myosin VII and talin A form a complex and are required for adhesion of cells to the substratum (Fig. 3 B; Niewohner et al., 1997; Tuxworth et al., 2005). We examined whether the overexpression of Rap1^{G12V} could bypass the *talin A*–null cell defects. Overexpressing Rap1^{G12V} in *talin A*–null cells

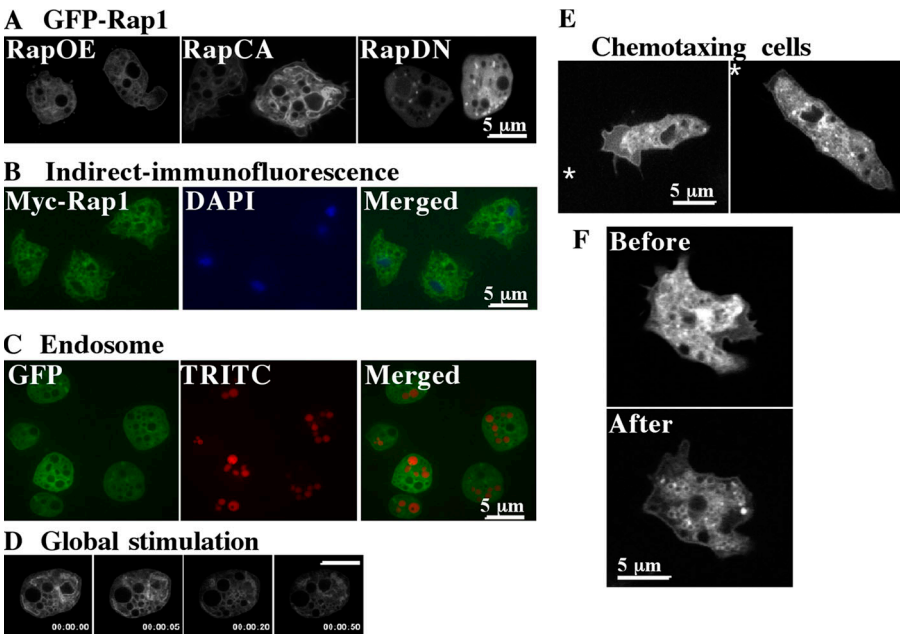

Figure 2. **Localization of Rap1.** (A) GFP-Rap1 in living cells. KAx-3 cells expressing GFP-Rap1 (RapOE), GFP-Rap1^{G12V} (RapCA), or GFP-Rap1^{S17N} (RapDN) were placed on glass coverslips and imaged with a laser-scanning confocal microscope. (B) Myc-Rap1 by indirect immunofluorescence. Cells expressing myc-Rap1 proteins were fixed with 3.7% formaldehyde and stained with anti-myc antibodies. Nuclei were visualized with DAPI. (C) GFP-Rap1 on the endosomal membrane. Fluid-phase endosomes in the cells expressing GFP-Rap1 proteins were labeled with TRITC-dextran. Dual-color confocal images were acquired. (D) Fluorescent images of an aggregation-competent cell expressing GFP-Rap1 after uniform chemoattractant stimulation. Bar, 5 μm. (E) GFP-Rap1 in the migrating cells. The asterisks indicate the direction of the micropipette. (F) GFP-Rap1 after the removal of cytoplasm. The soluble cytoplasm of cells expressing GFP-Rap1 was removed by breaking the plasma membrane using a micropipette under a microscope. Images from the same cell were taken before or after removal of the cytoplasm.

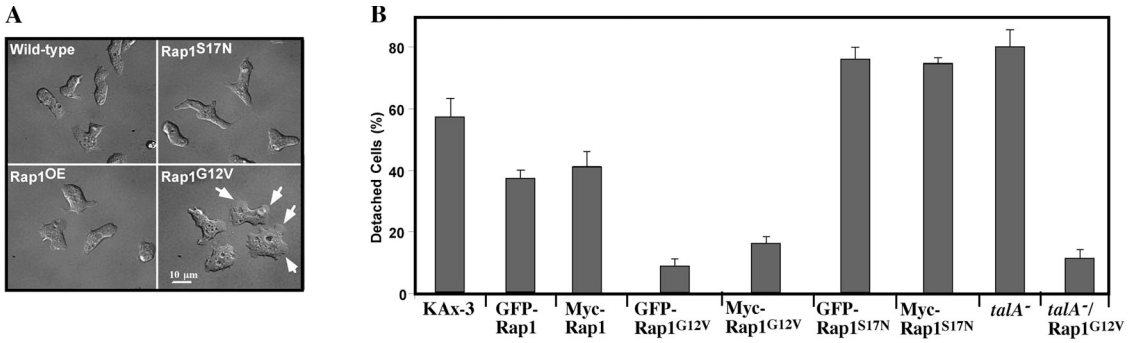

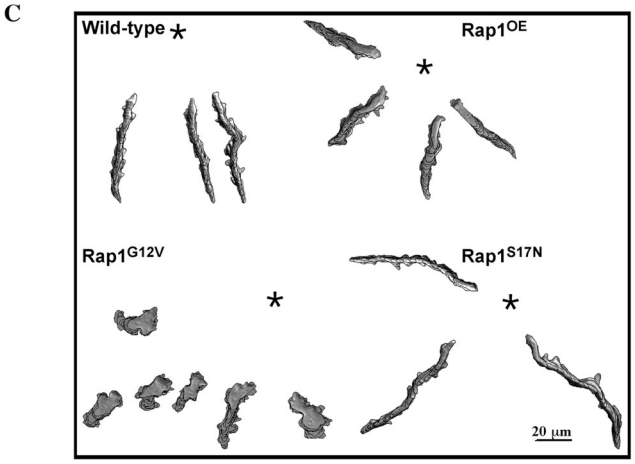

Strain	Speed (μm/min)	Directionality	Direction Change (deg)	Roundness (%)	Pseudopod number
Wild-type (KAx-3)	8.88 ± 0.60	0.80 ± 0.06	24.8 ± 2.6	44.7 ± 2.3	1.4± 0.68
MycRap1-OE	6.00 ± 0.17	0.64 ± 0.04	41.8 ± 5.2	47.5 ± 4.4	1.7± 0.91
MycRap1-G12V	3.54 ± 0.44	0.14 ± 0.02	77.7 ± 1.5	48.1 ± 3.8	3.2± 1.5
MycRap1-S17N	9.11 ± 0.55	0.82 ± 0.02	22.9 ± 1.7	45.3 ± 5.3	1.4± 0.75

Figure 3. **Rap1 effects on cell morphology, adhesion, and chemotaxis.** (A) Cell spreading by active Rap1. Aggregation-competent cells expressing myc-Rap1 proteins. Arrows indicate flattened and spread edges of the cells expressing Rap^{G12V}. (B) Cell-substratum adhesion assays were performed as described in Materials and methods. Adhesion was measured by the ratio of detached cells compared with the total number of cells. Experiments were performed at least three times. Error bars represent SD. (C) Chemotaxis of the cells expressing Rap1. Cells were traced from the videos and analyzed using DIAS software. Representative stacked images are shown. Images taken every minute were superimposed. The asterisks indicate the positions of a micropipette containing cAMP. The results of DIAS analysis are shown in the table. Speed indicates the speed of the cell's centroid movement along the total path. Directionality is a measure of how straight the cells move, and direction change is a measure of the number and frequency of turns the cell makes. Roundness is an indication of the polarity of the cells. The number of newly formed pseudopodia was counted in every 6-s image for the 10-min time period.

results in cells with a strong substratum attachment similar to that of wild-type cells overexpressing Rap1^{G12V}. This suggests that either Rap1 lies downstream of myosin VII–talin A or Rap1 and myosin VII–talin A function in distinct pathways to control attachment and that Rap1^{G12V} can promote attachment independently of talin A.

Wild-type cells become polarized and chemotax to a micropipette emitting the chemoattractant cAMP with a high speed and chemotaxis index, an indicator of the directionality of movement (Fig. 3 C). Rap1^{G12V} cells move at <50% of the speed of wild-type cells and have a substantially decreased chemotaxis index resulting from the production of lateral pseudopodia (and an increased number of turns) and the decreased formation of a prominent leading edge in the direction of the chemoattractant gradient (Fig. 3 C and Fig. S2, available at http://www.jcb.org/cgi/content/full/jcb.200607072/DC1). Rap1^{OE} cells have a milder phenotype; Rap1^{S17N} has a speed and directionality similar to that of wild-type cells, although with a reduced number of turns and lateral pseudopodia (Fig. 3 C). Myc-Rap1^{OE} and myc-Rap1^{G12V} cells experience delayed multicellular development as a result of a delay in aggregation and morphogenesis. The aggregates are also smaller than those of wild-type cells (Fig. S3). In contrast, Rap1^{S17N} cells develop more rapidly than wild-type cells.

Rap1 control of myosin and the cell cortex

Wild-type cells rapidly round up and contract after treatment with azide (NaN_3) as described previously (Fig. 4 A; Pasternak et al., 1989; Kang et al., 2002). As shown in Fig. 4 A, cells overexpressing Rap1^{G12V} do not change shape after NaN_3 treatment, and, in agreement with a previous study, NaN_3-mediated contraction does not occur in cells lacking myosin II (*mhcA*$^-$ cells; Pasternak et al., 1989), suggesting an essential role for myosin II in this response. Fig. 4 (A and B) indicates that *mhcA*$^-$ (*myosin II* null) cells exhibit a flattened, spread shape and a high degree of substratum attachment compared with wild-type cells. The attachment of *mhcA*$^-$ cells is further increased by overexpressing Rap1^{G12V}. These results suggest that Rap1 functions through myosin II and other pathways to control cell adhesion.

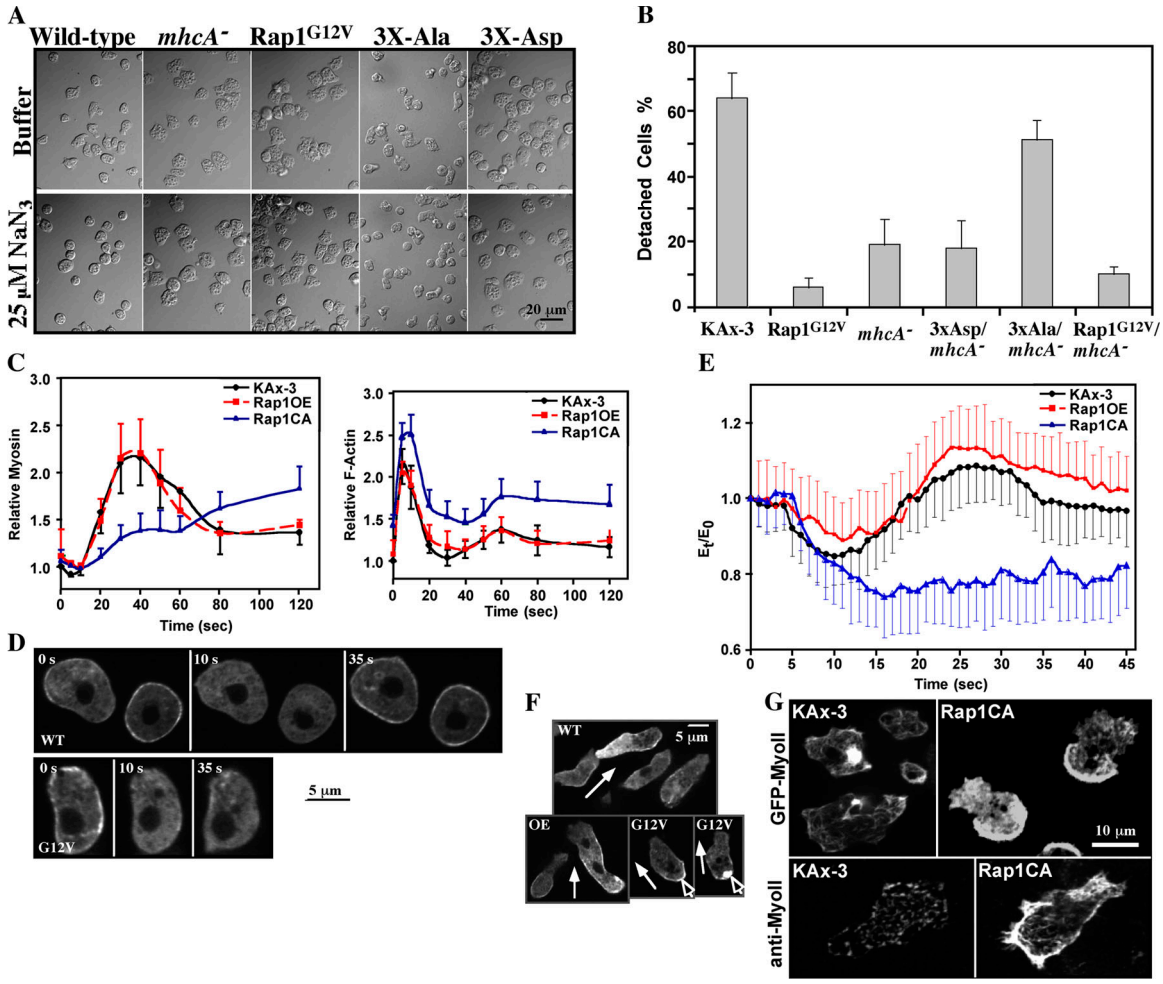

Figure 4. **Rap1 control of myosin and the cell cortex.** (A) Cell morphology after NaN_3 treatment. Log-phase vegetative wild-type cells, cells expressing $Rap1^{G12V}$, *mhca*-null cells (*mhcA*$^-$), and *mhca*-null cells expressing the myosin heavy chain phosphorylation mutant 3XAsp or 3XAla were washed with oxygenated MES buffer and treated with sodium azide. (B) Cell adhesion assay of *mhcA* mutants in the presence of NaN_3. (C) Kinetics of F-actin polymerization and myosin II assembly in the Triton X-100–insoluble cytoskeletal fraction of wild-type cells and cells expressing myc-Rap1 in response to chemoattractant stimulation. (D) Delocalization and relocalization of GFP–myosin II to the cell cortex in response to uniform cAMP stimulation. GFP–myosin II was coexpressed with myc-Rap1 proteins in wild-type KAx-3 cells. Cells were stimulated with cAMP, and the fluorescence images were taken every second. Three representative frames are shown. (E) The fluorescence intensity of membrane-localized GFP–myosin II was quantitated as in Fig. 1 C. Error bars represent SD. (F) Localization of GFP–myosin II in the migrating cells coexpressing myc-Rap1 proteins. Arrows indicate the direction of movement, and arrowheads indicate the GFP–myosin II–concentrated region in the cells expressing Rap^{G12V}. (G) Localization of GFP–myosin II on the bottom of cells coexpressing myc-$Rap1^{G12V}$ was visualized by confocal microscope (top). To visualize the endogenous myosin II at the bottom of the cells, membrane cytoskeletons attached on the glass coverslips were prepared as described by Yumura and Kitanishi-Yumura (1992). Cells expressing $Rap1^{G12V}$ were placed on the polylysine-coated glass coverslips and immunostained with anti–myosin II antibodies after removal of the top part of cell bodies. The same exposures were used for the images.

Myosin II assembly in *D. discoideum* is regulated by the differential phosphorylation of three Thr residues ($Thr^{1,823}$, $Thr^{1,833}$, and $Thr^{2,029}$) in the myosin II tail by a family of myosin II heavy chain kinases (MHCKs; Pagh et al., 1984; Egelhoff et al., 1993; De la Roche et al., 2002; Yumura et al., 2005). Unphosphorylated myosin II self-assembles, whereas myosin II is disassembled in vivo by phosphorylation by the MHCKs. Substitution of $Thr^{1,823}$, $Thr^{1,833}$, and $Thr^{2,029}$ with alanines (3XAla) leads to overassembled myosin II, whereas Asp substitutions (3XAsp) cause constitutively unassembled myosin II. As expected, *mhcA*$^-$ cells expressing myosin II^{3XAsp} behave similarly to *mhcA*$^-$ cells: they exhibited high attachment, are spread, and do not change shape upon NaN_3 treatment (Fig. 4, A and B). In contrast, *mhcA*$^-$ cells expressing myosin II^{3XAla} are more rounded before NaN_3 treatment and do not round further upon NaN_3 treatment (Fig. 4 A), presumably because they are already contracted. These cells also exhibit less adhesion (Fig. 4 B).

Because of the similarity of phenotypes and properties of *mhcA*$^-$ cells and cells expressing $Rap1^{G12V}$, we investigated the effect of Rap1 on the reorganization of the cytoskeleton in response to chemoattractant stimulation. In wild-type cells, chemoattractant stimulation results in a rapid, transient phosphorylation of myosin II, causing a small but reproducible drop in assembled myosin II in the Triton X-100 pellet after ~5–10 s (Fig. 4 C). This response is followed by an ~2.0–2.5-fold increase in cortical myosin II that peaks at ~40 s (Liu and Newell, 1991; Steimle et al., 2001; Park et al., 2004). Myosin II assembly is not visibly affected by overexpressing wild-type Rap1.

However, the overexpression of Rap1^{G12V} causes a major alteration in chemoattractant-stimulated changes in assembled myosin II. After the small decrease in cortical myosin II levels, there is only a slight and gradual rise in assembled myosin II that reaches a first plateau of ~20% of the level of myosin II in wild-type cells at 40 s, the time when assembled myosin II levels peak in wild-type cells (Fig. 4 C). There is a secondary, slow rise in assembled myosin II after 60 s, reaching a level of ~50–60% of that of assembled myosin II in wild-type cells at 120 s. The response in wild-type cells returns to near basal levels by 80 s.

We used GFP–myosin II expressed in *mhcA*$^-$ cells, which complements *mhcA*$^-$ cell defects, to examine the changes in cortically localized myosin II in resting cells and in response to chemoattractant stimulation (Levi et al., 2002; Bosgraaf et al., 2005). Unstimulated cells exhibit a basal level of GFP–myosin II at the cell cortex (Fig. 4, D and E). Upon chemoattractant stimulation, after a lag of a few seconds, there is a decrease in GFP– myosin II at the cortex with a minimum at ~10 s followed by an increase to above basal levels with a broad peak centered at 25–30 s and a subsequent decrease to basal levels. Rap1^{OE} cells have a similar response.

As with the assay that quantifies myosin II in the Triton X-100–insoluble fraction, Rap1^{G12V} cells exhibit an abnormal GFP–myosin II response (Fig. 4, D and E). At 5 s after stimulation, the level of cortical GFP–myosin II decreases substantially. Although a minimum is reached at ~10 s in wild-type cells, the level of cortical GFP–myosin II continues to decrease in Rap1^{G12V} cells with a low point at 15–20 s. Levels increase only slightly through 45 s. These data are consistent with a delayed and weak chemoattractant-mediated cortical accumulation of myosin II in cells overexpressing Rap1^{G12V}. Our findings suggest that Rap1 directly or indirectly negatively regulates myosin II assembly at the cell cortex.

We used GFP–myosin II to study the spatial localization of myosin II in unstimulated vegetative cells and in developed cells chemotaxing to a micropipette. Wild-type cells have some cortically localized GFP–myosin II, and some cells have small patches of myosin II (Fig. 4 F). In contrast, vegetative Rap1^{G12V} cells are highly polarized, with one pole exhibiting a broad domain of GFP–myosin II concentrated along the cortex. The other pole has a ruffled front similar to what is sometimes observed at the leading edge of chemotaxing cells. We found that although wild-type cells have a very low level of myosin II

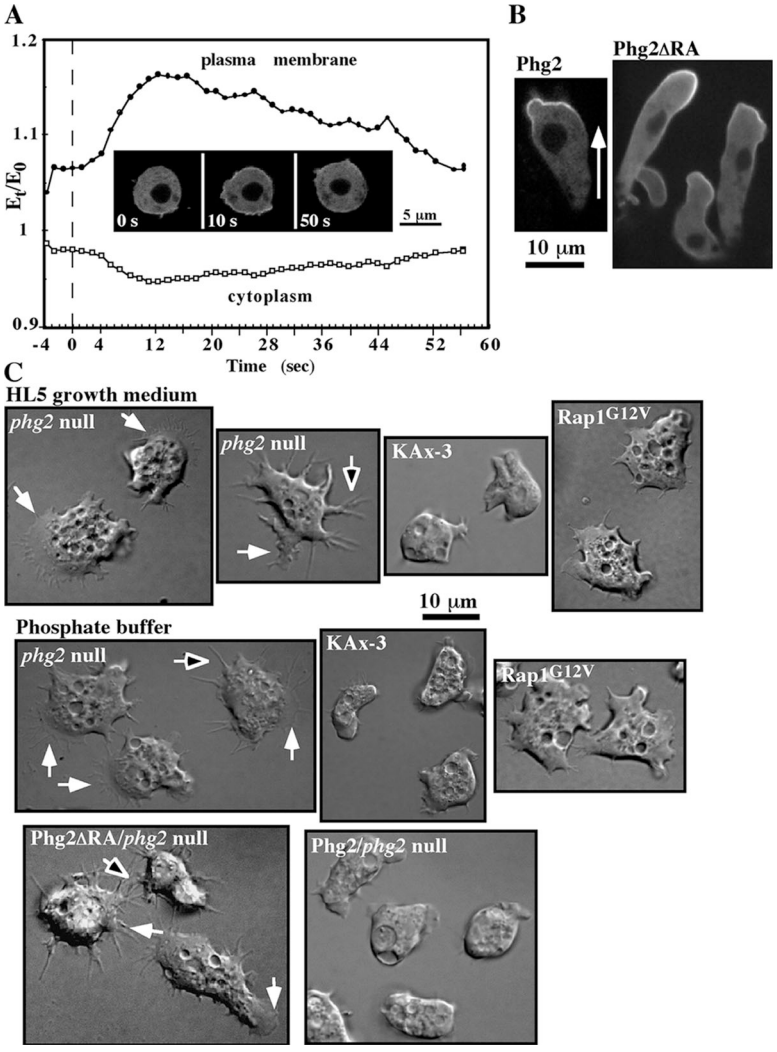

Figure 5. **Subcellular localization of GFP-Phg2 and morphology of *phg2*-null cells.** (A) Translocation of GFP-Phg2 to the cell cortex in response to cAMP stimulation. The fluorescence intensity on the plasma membrane fraction or in the cytosol fraction was quantitated using SimplePCI Imaging Systems. The graphs represent mean values of 10 cells from two separate experiments. (B) Localization of GFP-Phg2 in the migrating cells. The arrow indicates the direction of movement. (C) Morphology of *phg2*-null cells. Vegetative cells were plated in HL5 growth medium or Na/K phosphate buffer on a plate with a hole covered by a glass coverslip and were imaged. *phg2*-null cells show lamellipodia-like (white arrows) or filopodia-like structures (black arrows) compared with wild-type cells.

(endogenous myosin II or GFP–myosin II) along the bottom of cells (Fig. 4 G), Rap1^{G12V} cells have a highly polarized myosin II localization along one pole of the cell. In chemotaxing wild-type cells, myosin II localizes to the posterior and along the lateral sides toward the cell's posterior as reported previously (Clow and McNally, 1999). In Rap1^{G12V} cells, much of the myosin II is found in a highly localized region at the very posterior of cells. These findings suggest that Rap1 may be involved in spatially restricting myosin II away from the leading edge in polarized cells.

Wild-type cells exhibit a biphasic F-actin polymerization profile with a sharp peak at 5 s and a second, lower, and broader peak at ∼45–60 s that has been linked to pseudopod extension (Fig. 4 C; Hall et al., 1989). Overexpressing Rap1^{G12V} results in an ∼40% increase in the basal level of F-actin. The kinetics of the response are similar to those of wild-type cells, with the level of F-actin proportionally higher in Rap1^{G12V} cells as a result of the higher basal level of F-actin in unstimulated cells. The overexpression of wild-type Rap1 has little effect on the F-actin profile.

Regulation of Phg2, a Rap1 effector

The Phg2 Ser/Thr kinase was identified in a genetic screen for genes required for phagocytosis (Gebbie et al., 2004) and was identified independently by us in a yeast two-hybrid screen for proteins that interact with the PH domain–containing protein PhdB. Phg2 has an N-terminal PI(4,5)P_2-binding domain, a Rap1-GTP–binding RA domain, and a Ser/Thr kinase domain and colocalizes with F-actin protrusions in vegetative cells (Gebbie et al., 2004; Blanc et al., 2005). We confirmed that the Phg2 RA domain preferentially binds Rap1-GTP over Ras-GTP (Gebbie et al., 2004; unpublished data).

We examined the subcellular localization of Phg2 using a GFP fusion (see Materials and methods). Fig. 5 A indicates that GFP-Phg2, which complements the *phg2*-null phenotypes (not depicted), exhibits a low level of cortical localization in unstimulated cells. Upon chemoattractant stimulation, GFP-Phg2 rapidly and transiently translocates to the cell cortex. The level of cortical Phg2 peaks at ∼10 s. Phg2 localizes to the leading edge of polarized chemotaxing cells, with the localization extending weakly toward the posterior (Fig. 5 B). Thus, Phg2 shows a temporal and spatial localization similar to that of Rap1-GTP. This contrasts with Ras-GTP and PH domain proteins (e.g., CRAC and Akt/PKB) that are highly restricted to the leading edge and are absent from the lateral sides of chemotaxing cells (Sasaki et al., 2004). To determine whether the RA domain is required for the leading edge localization of Phg2 in chemotaxing cells, we created GFP-Phg2ΔRA, a Phg2 construct lacking the RA domain. In chemotaxing cells, the localization of GFP-Phg2ΔRA was similar to that of GFP-Phg2, indicating that the RA domain is not required for Phg2 localization (Fig. 5 B). We also studied the possible mechanisms by which Phg2 is recruited to the cortex. The localization is unaffected in cells treated with LY294002 and in cells lacking PI3K1 and PI3K2 (*pi3k1/2*-null cells) nor is localization affected by pretreatment with the actin inhibitor latrunculin A (unpublished data). These results suggest that Phg2 localization is not controlled by the PI3K or F-actin pathways that mediate the leading edge localization of several signaling components involved in the formation of a stable leading edge (Sasaki and Firtel, 2006).

To investigate the function of Phg2, we created a *phg2*-null strain in our wild-type strain KAx-3 (see Materials and methods; unpublished data). *phg2*-null cells in either HL5 axenic growth medium or phosphate buffer are very flat and spread compared with wild-type cells (and are not multinucleated) and, like Rap1^{G12V} cells, often have large lamellipodia-like structures on one side of the cell (Rap1^{G12V} cells are shown as a comparison; Fig. 5 C). The cells often have numerous and more prominent filipodia-like structures compared with wild-type cells, which are not observed in Rap1^{G12V} cells. The phenotypes were complemented by expressing GFP-Phg2 but not GFP-Phg2ΔRA. Collectively with the localization of GFP-Phg2ΔRA, these data suggest that the RA domain and presumably Rap1-GTP are required for Phg2 function but not its localization. We created a second *phg2*-null strain in which the Bsr selection cassette was inserted in the opposite orientation. Both *phg2*-null strains had similar phenotypes that were complemented by expressing tagged wild-type Phg2 (unpublished data).

Phg2 is required for regulation of cell adhesion and chemotaxis

Previous studies determined that *phg2*-null cells exhibit defects in particle binding, cell attachment, and basal cell motility when assayed in HL5 axenic growth medium (Gebbie et al., 2004). We confirmed a decrease in the rate of phagocytosis in our *phg2*-null strain (unpublished data). Our *phg2*-null strain exhibited a very strong increase in cell attachment compared with our parental wild-type cells (Figs. 6 A and S1). These phenotypes were complemented by the expression of tagged Phg2 in the *phg2*-null strain. There are conflicting data concerning the cell adhesion of *phg2*-null cells. Gebbie et al. (2004) found that their *phg2*-null cells in a DH1 background exhibited ∼90% less adhesion compared with wild-type cells as assayed in a flow chamber. Using a plate-shaking assay, Kortholt et al. (2006) showed that the same strain had a mildly reduced adhesion. To confirm our data and to directly compare the two strains, we measured cell adhesion in the plate-shaking assay of Kortholt et al. (2006) (Fig. S1). These findings confirmed both our results and those of Kortholt et al. (2006) and demonstrated an intrinsic difference between the two *phg2*-null strains and parental backgrounds. Our *phg2*-null strain phenotypes are fully complemented by GFP-Phg2, indicating that the phenotypes result from the disruption of Phg2. Chemotaxing *phg2*-null (*phg2*$^{KAx\text{-}3^-}$) cells exhibit strong chemotaxis phenotypes. The cells move slower than wild-type cells, have a broader leading edge than wild-type cells, and produce numerous dominant lateral pseudopodia and more pronounced smaller projections from the leading edge (Fig. 6, B–D). These phenotypes are complemented by expressing GFP- or GST-Phg2 in *phg2*-null cells.

As shown in Fig. 6 E and Fig. S4 (available at http://www.jcb.org/cgi/content/full/jcb.200607072/DC1), F-actin levels were ∼1.5-fold higher in unstimulated *phg2*-null cells compared with those in wild-type cells. Upon chemoattractant stimulation,

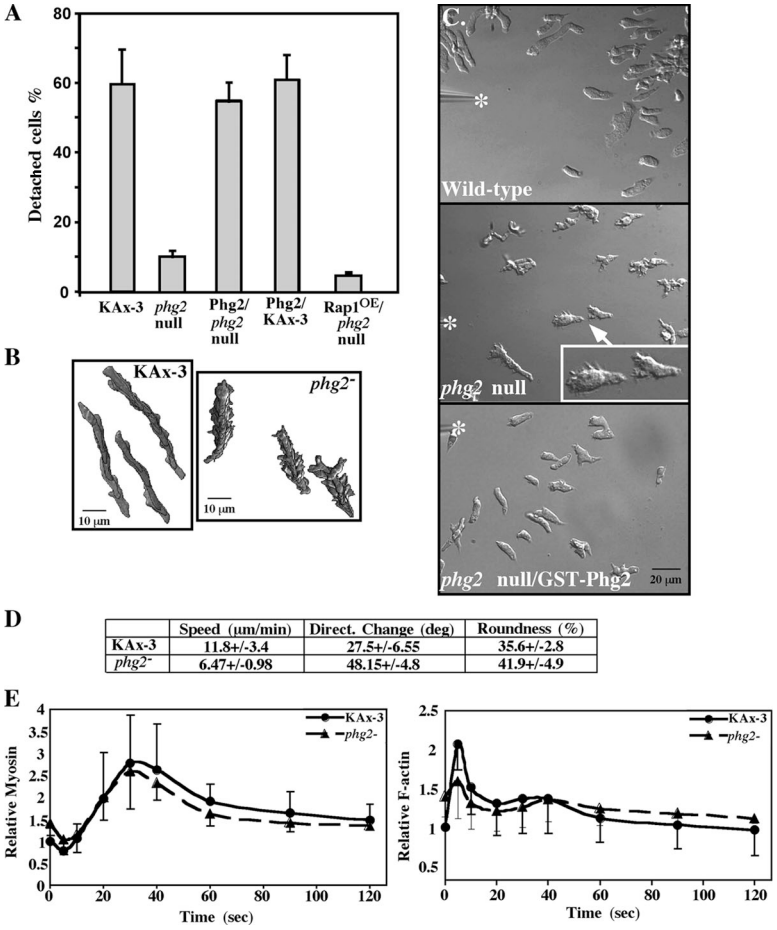

Figure 6. **Regulation of cell adhesion and chemotaxis by Phg2.** (A) Cell adhesion of *phg2* mutants. (B) Chemotaxis of *phg2*-null cells. Cells were traced and analyzed as in Fig. 3 C. Superimposed images of representative traces of wild-type KAx-3 and *phg2*-null strains are shown. The superimposed images show the cell shape, direction, and length of the path at 1-min intervals. (C) Representative frames from chemotaxis videos of wild-type cells, *phg2*-null cells, and *phg2*-null cells expressing GST-Phg2. The inset in the middle panel shows an enlargement of two representative cells (arrow). Asterisks indicate the positions of the micropipette containing cAMP. (D) DIAS analysis of chemotaxis. (E) Kinetics of F-actin polymerization and myosin II assembly in the Triton X-100–insoluble cytoskeletal fraction of wild-type cells and *phg2*-null cells. Error bars represent SD.

phg2-null cells showed only a small first peak of F-actin polymerization relative to wild-type cells, which had a 2.2-fold increase. A small second peak was observed at ∼40 s. This overall reduced level of F-actin polymerization might account for the reduced speed of *phg2*-null cell chemotaxis. Unstimulated *phg2*-null cells had ∼30% more myosin II in the Triton X-100 pellet compared with wild-type cells (Fig. 6 E). Upon stimulation, *phg2*-null cells exhibited a small decrease in myosin II levels at ∼5 s and a subsequent peak at ∼40 s, which were changes similar to those in wild-type cells.

Our F-actin and myosin II assays used developed cells that are stimulated in suspension, whereas our attachment assays were performed with vegetative cells adhered to a substratum. Therefore, we examined whether the differences in the basal levels of F-actin and cortical myosin II between strains found in suspension assays are also representative of adherent cells. As depicted in Fig. S4, the data are similar to those obtained from developed cells in suspension.

Phg2 is required for cortical myosin II phosphorylation in vitro

To study the regulation of myosin II associated with the cortex in *phg2*-null cells, we examined the spatial-temporal localization of GFP–myosin II in vivo. Myosin II does not delocalize from the cortex in response to chemoattractant stimulation (unpublished data). As myosin II dissociation depends on myosin II phosphorylation (De la Roche et al., 2002), this observation suggested that Phg2 might regulate myosin II phosphorylation.

Gebbie et al. (2004) demonstrated that the expression of Phg2 in *Escherichia coli* led to the in vivo phosphorylation of bacterial proteins on Ser/Thr residues, indicating that Phg2 has Ser/Thr kinase activity. However, Phg2 purified from bacteria did not exhibit kinase activity under the conditions assayed. To examine Phg2 kinase activity, we expressed GFP- and GST-tagged Phg2 in *phg2*-null cells and found that both proteins complemented the Phg2 chemotaxis and attachment defects. Triton X-100 lysates of cells before and at various times after chemoattractant stimulation were fractionated into soluble (10K supernatant) and insoluble (cortical) fractions, which were assayed for potential Phg2 activity. For the soluble fraction, we purified Phg2 (GFP-Phg2 by immunoprecipitation and GST-Phg2 on glutathione–Sepharose beads) and assayed for kinase activity using myelin basic protein or histone 2B as substrates. No activity was observed (unpublished data). We assayed the insoluble/cortical fraction similarly and detected no activity on exogenous substrates (unpublished data). We studied Phg2 activity indirectly in the cortical fraction by assaying kinase activity against endogenous substrates by incubating the Triton X-100–insoluble pellet with Mg^{2+}–γ- [^{32}P]ATP and comparing samples from wild-type and *phg2*-null cells. We observed a single [^{32}P]O_4-labeled band (of ∼250 kD) in samples from wild-type cells that was not observed in samples from *phg2*-null

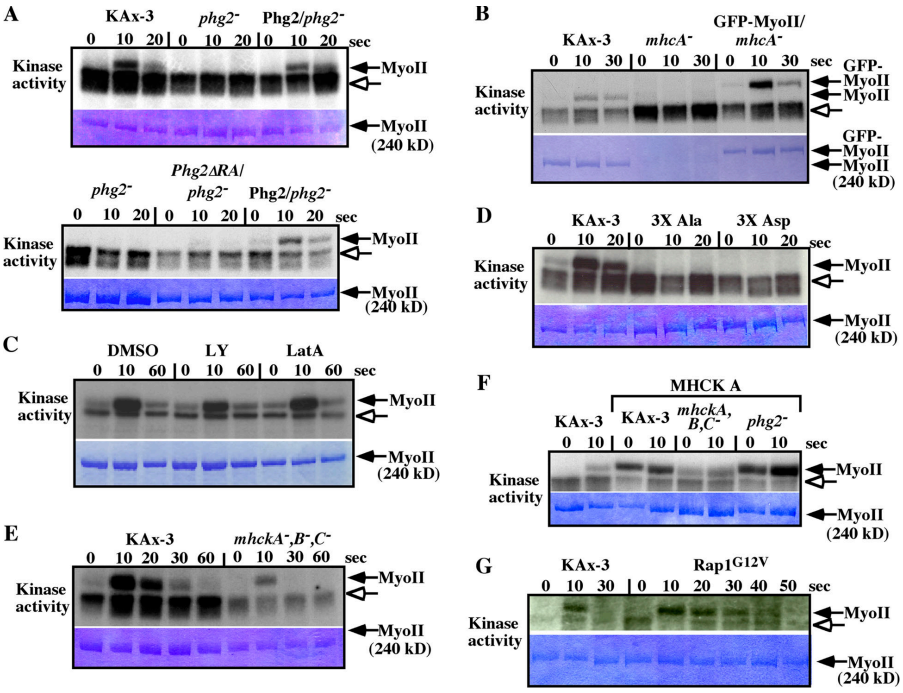

Figure 7. **Cortical myosin II phosphorylation by Phg2.** The cytoskeletal fractions from cells at the indicated times after cAMP stimulation were assayed for kinase activity (see Materials and methods). The reactions were subjected to SDS-PAGE and were Coomassie blue stained (bottom panel of each figure). The top panel of each figure shows an autoradiogram of the gel depicted in the bottom panel. Solid arrows indicate the position of myosin II, and open arrows point to bands of unknown composition. (A) Assay of wild-type, *phg2*-null, and *phg2*-null cells expressing Phg2 or Phg2ΔRA. (B) Assay of *mhca*-null cells and *mhca*-null cells expressing GFP–myosin II. (C) Assays in which cells were pretreated with latrunculin A or LY294002 for 20 min before stimulation. Control cells were treated with DMSO, the solvent for the two drugs. (D) *mhca*-null cells expressing myosin II^{3XAla} or myosin II^{3XAsp}. (E) *mhck-A*$^-$, *-B*$^-$, and *-C*$^-$ cells. (F) Cells expressing MHCK-A. (G) $Rap1^{G12V}$-expressing cells.

cells (Fig. 7 A; the remainder of the gel is not depicted). The band was barely detectable in samples from unstimulated cells, strong in samples from cells stimulated for 10 and 20 s, and barely detectable in samples from later time points. As the band is not observed in *phg2*-null cells, we suggest that Phg2 is required for phosphorylation of the ~250-kD protein in this assay. The kinase activity is restored in *phg2*-null cells expressing wild-type Phg2 but not GFP-Phg2ΔRA, suggesting that the RA domain is required for Phg2 activity and that Phg2 activity may be activated by Rap1-GTP. Our assay does not distinguish between Phg2 directly phosphorylating the ~250-kD protein or being required for the activity of another kinase that directly phosphorylates myosin II.

Coomassie blue–stained gels showed that the ~250-kD phosphorylated protein comigrated with the myosin II band. To examine the possibility that the phosphorylated band is myosin II, we repeated the assay in *mhcA*$^-$ cells and found that the band was absent (Fig. 7 B). To distinguish between the protein being myosin II and it requiring myosin II for its cortical localization, we expressed GFP–myosin II in *mhcA*$^-$ cells. The phosphorylated band was then present, and its mobility corresponded to GFP–myosin II (Fig. 7 B), indicating that the phosphorylated protein is myosin II. This activity was unaffected by pretreatment with LY294002 or latrunculin A, which is consistent with our findings that Phg2 cortical localization is unaffected by the treatment of these drugs and indicating that these pathways were not dependent on the PI3K pathway or F-actin polymerization (Fig. 7 C).

We then assayed *mhcA*$^-$ cells expressing myosin II^{3XAla} or myosin II^{3XAsp} to examine whether $Thr^{1,823}$, $Thr^{1,833}$, or $Thr^{2,029}$ might be the sites of myosin II phosphorylation. Fig. 7 D illustrates that neither of these substituted myosin II proteins are phosphorylated. Although these findings are consistent with the sites of Phg2-dependent myosin II phosphorylation being $Thr^{1,823}$, $Thr^{1,833}$, or $Thr^{2,029}$, we cannot exclude the possibility that $Thr^{1,823}$, $Thr^{1,833}$, or $Thr^{2,029}$ are not the sites of phosphorylation and that the actual sites of phosphorylation are unavailable in myosin II^{3XAla} and myosin II^{3XAsp} in our assay for an unknown reason. We also investigated myosin II phosphorylation in cells lacking three of the four MHCKs (*mhck-A*/*-B*/*-C*–null cells), which exhibit an extensive myosin II overassembly (Yumura et al., 2005). Fig. 7 E indicates that myosin II phosphorylation is highly reduced in this strain, suggesting that the myosin II phosphorylation pathway requires MHCK. The overexpression of MHCK-A in *phg2*-null cells suppresses the lack of myosin II phosphorylation in our assay (Fig. 7 F). The kinase activity is found in unstimulated as well as stimulated cells, with the activity increasing after stimulation. We find that as previously reported for wild-type cells (Steimle et al., 2001), MHCK-A localizes to the leading edge of chemotaxing *phg2*-null cells, suggesting that the loss of myosin II kinase activity in *phg2*-null cells is not caused by the inability to recruit MHCK-A (unpublished data). Phg2 has a Rap1-GTP–binding RA domain and, therefore, is expected to lie downstream from Rap1. Cells expressing Rap1G12V have an elevated level of myosin II phosphorylation that is also extended, which is consistent with increased and extended activation mediated by the activated form of Rap1 (Fig. 7 G).

Discussion

Rap1 regulates myosin II assembly and cell adhesion

We demonstrated that Rap1 is dynamically activated in response to chemoattractant stimulation with a Rap1-GTP GFP reporter transiently localizing to the cell cortex with a peak at 5–10 s. In chemotaxing cells, activated Rap1 is found predominantly at

the leading edge of chemotaxing cells with a distribution that weakly extends along the cortex toward the posterior, whereas total Rap1 is found predominantly on membrane vesicles and along the plasma membrane, as in mammalian cells. The spatial distribution of Rap1-GTP extends more laterally than that of Ras-GTP, and the kinetics of activation are slower, suggesting that the sites of function of Rap1 and Ras overlap but are not coincident.

$Rap1^{G12V}$ cells are very flat and adherent to the substratum, which is consistent with findings in mammalian cells, indicating the involvement of Rap1 in controlling cell shape and attachment. These cells chemotax slowly and produce numerous lateral pseudopodia, probably in part because they cannot regulate their attachment to the substratum and restrict the activation of pseudopod formation to the side of the cell closest to the chemoattractant source. $Rap1^{S17N}$ cells have a modest reduction in attachment. The $Rap1^{S17N}$ phenotypes are weak, presumably because $Rap1^{S17N}$ does not effectively inhibit the Rap1 GEFs, as there is little change in the activation of endogenous Rap1 in these cells.

Our studies suggest that one mechanism by which Rap1 controls cell spreading and attachment in *D. discoideum* acts at least partially through the regulation of myosin II assembly. $Rap1^{G12V}$ cells exhibit weak chemoattractant-mediated myosin II assembly, which is consistent with an inability to control cell contraction. In response to NaN_3 treatment, wild-type but not $Rap1^{G12V}$ cells contract, which is consistent with previous studies (Pasternak et al., 1989; Kang et al., 2002). These phenotypes are shared by cells lacking myosin II (*mhcA*$^-$ cells) or *mhcA*$^-$ cells expressing myosin II^{3XAsp}. These strains exhibit a spread, flat cell shape and a high substratum attachment. In $Rap1^{G12V}$ cells, GFP–myosin II dissociates from the cell cortex in response to chemoattractant stimulation but undergoes only a slight and greatly delayed reassociation with the cortex. $Rap1^{G12V}$ cells exhibit an abnormal and deeply reduced chemoattractant-mediated myosin II assembly with slow kinetics. These findings suggest that Rap1 negatively controls myosin II assembly.

MHCKs are the major kinases that phosphorylate myosin II on $Thr^{1,823}$, $Thr^{1,833}$, and $Thr^{2,029}$ and result in myosin II disassembly (Egelhoff et al., 1993; De la Roche et al., 2002). MHCK-A is recruited to the leading edge by binding to F-actin, which activates the kinase (Egelhoff et al., 2005), thereby disassembling myosin II at the site of leading edge protrusion. Our findings that Rap1 is activated at the leading edge and that the expression of $Rap1^{G12V}$ causes extended myosin II disassembly suggest that Rap1 may be a key upstream spatial regulator of myosin II assembly. We suggest that Rap1 may prevent myosin II assembly at the leading edge and may indirectly (passively) promote its assembly at the posterior of cells. Myosin II assembly and phosphorylation are regulated by cGMP in *D. discoideum* (Bosgraaf et al., 2002, 2005; Bosgraaf and van Haastert, 2006). Cells lacking the cGMP-binding protein GbpC exhibit a spatial-temporal profile of GFP–myosin II cortical disassembly/assembly similar to that of $Rap1^{G12V}$ cells. The profile of myosin II in the Triton X-100–insoluble pellet is similar to that of cells lacking both guanylyl cyclases (Bosgraaf et al., 2002, 2005). Thus, cells expressing $Rap1^{G12V}$ exhibit phenotypes similar to those lacking cGMP or the cGMP effector GbpC, suggesting that Rap1 may be a negative regulator of the cGMP pathway. Just before submission of this manuscript, a study by Kortholt et al. (2006) demonstrated that GpbD is a Rap1 GEF and that its overexpression leads to increased cell adhesion and chemotaxis defects similar to those of the $Rap1^{G12V}$ cell presented here. They present evidence that Rap1 lies upstream of Phg2.

Our model by which Rap1 may control anterior and posterior functions may be analogous to the proposed mechanism by which anterior and posterior functions are differentially regulated by Gαi and Gα12/13 in neutrophils (Wong et al., 2006). Gαi promotes the leading edge function and inhibits posterior function (activation of RhoA and assembly of myosin II), whereas Gα12/13 controls posterior functions by mediating RhoA activation. The loss of Gαi function increases RhoA activity, whereas the inhibition of RhoA function increases leading edge function, indicating that the regulation of anterior and posterior functions is balanced. In *D. discoideum*, anterior and posterior functions have different response kinetics and are spatially restricted in polarized cells (Van Haastert and Devreotes, 2004; Sasaki and Firtel, 2006). Chemotaxing $Rap1^{G12V}$ cells often have a flat, extended posterior region that does not lift from the substratum, suggesting that Rap1 plays a part in controlling the posterior function of moving cells. In addition, the localization of myosin II is altered in unstimulated $Rap1^{G12V}$ compared with wild-type cells. Although myosin II has a general localization along the cortex except at sites of pseudopod extension with an enrichment at the posterior in wild-type cells (Clow and McNally, 1999), resting $Rap1^{G12V}$ cells have a polarized cytoskeletal organization with myosin II present in a single, extended domain along approximately one third of the cortex opposite a domain that has the appearance of a projecting lamellipod. In chemotaxing $Rap1^{G12V}$ cells, myosin II is found almost exclusively in a small cap/domain at the posterior of cells, as though myosin II sites are restricted from other areas of the cell through the constitutive activation of Rap1. This lack of visible myosin II along the cell's lateral sides may contribute to a possible loss of myosin II–mediated cortical tension and the presence of lateral pseudopodia.

Role of Phg2

We demonstrated that Phg2 is a key regulator of the cell's cytoskeleton and cell attachment. *phg2*-null cells are highly adhesive, which is a finding that contrasts that of Gebbie et al. (2004). We discovered that under two different assay conditions, their *phg2*-null strain has increased adhesion in phosphate buffer, suggesting that differences may be caused by assay conditions. As *phg2*-null cells exhibit high adhesion, we suggest that Phg2 negatively regulates cell adhesion.

Phg2 is required for proper chemotaxis. Chemotaxing *phg2*-null cells move slowly and have a broad leading edge with numerous small protrusions. The broad leading edge structure (more of a lamellipod than a pseudopod) and protrusions are presumably related to the broad lamellipod and filopodia-like protrusions exhibited by vegetative *phg2*-null cells. These cells have reduced random motility (Gebbie et al., 2004; unpublished data). Phg2 leading edge localization does not require the RA

domain, but the ability to complement the null phenotypes does, indicating that the genetic function of Phg2 is dependent on Phg2's ability to bind Rap1-GTP. These findings demonstrate that Phg2 and, thus, its putative regulator Rap1 play key roles in controlling leading edge formation and in suppressing these lateral and adventitious protrusions. *phg2*-null cells have a deeply reduced F-actin response, which, along with the high attachment of these cells, may account for their reduced chemotactic speed.

A further understanding of the possible mechanism by which Phg2 controls the cytoskeleton was obtained by examining the physiological and biochemical phenotypes of *phg2*-null cells. *phg2*-null cells show an elevated basal level of myosin II and F-actin in vegetative and developmentally competent cells, which are normal kinetics of chemoattractant-mediated myosin II assembly, but show a substantially reduced F-actin polymerization response. Motile amoeboid cells (e.g., neutrophils and *D. discoideum*) spatially restrict F-actin polymerization and leading edge protrusion from myosin II assembly to the opposite poles of polarized cells (Van Haastert and Devreotes, 2004; Sasaki and Firtel, 2006; Wong et al., 2006). Myosin II thick filaments are partially responsible for cortical tension or rigidity. To protrude a pseudopod, cells must disassemble the myosin II thick filaments at that site. Our imaging data suggest that Phg2 is required for the disassembly of myosin II thick filaments; in the absence of Phg2, cells accumulate elevated levels of myosin II in the Triton X-100–insoluble fraction. We revealed that Phg2 is required for in vitro myosin II phosphorylation in a cortical fraction in response to chemoattractant stimulation. As this phosphorylation is thought to be responsible for myosin II disassembly from the cortex (De la Roche et al., 2002), our combined data suggest that Phg2 is required for efficient cortical myosin II phosphorylation and disassembly. We suggest that the defect in delocalizing myosin II from the cortex that we observe in *phg2*-null cells may be responsible for the restricted chemoattractant-mediated F-actin response. In $Rap1^{G12V}$ cells, myosin II disassembly is extended, and there is minimal reaccumulation over a 2-min time frame.

The initial responses observed after a global stimulation recapitulate the changes that occur at the leading edge of chemotaxing cells. Like other leading edge responses, Rap1 is activated rapidly at the cortex, and Phg2 translocates to the cortex in response to global stimulation. Rap1 is also activated at the leading edge, and Phg2 accumulates at this site. We suggest that Phg2 is a new component of the rapidly activated leading edge regulatory network that, in this case, controls myosin II phosphorylation and disassembly at this site. The reduced myosin II phosphorylation in *mhck-A*$^-$, *-B*$^-$, or *-C*$^-$ cells and constitutive activity in MHCK-A^{OE} cells suggest that this network may regulate MHCK-A (or other MHCKs), which localizes to the leading edge. The higher basal level of myosin II in *phg2*-null cells is consistent with this hypothesis. Phg2 may play other roles, as *phg2*-null cells have many cellular protrusions and extended lamellipodia in resting and chemotaxing cells, phenotypes that are not observed in cells lacking myosin II. *phg2*-null cells exhibit a normal myosin II response when one examines total myosin II that associates with the Triton X-100–insoluble fraction and are able to contract upon NaN_3 treatment. As such, we expect that *phg2*-null cells can assemble and disassemble myosin II in other domains of the cell. In conclusion, Rap1 is a major regulator of the cytoskeleton in resting cells and cells stimulated by chemoattractant or responding to osmotic stress, and it functions, at least in part, to control myosin II through Phg2. Therefore, Rap1 may be part of the signaling cascade by which leading edge and posterior functions of the cell interact to control cell polarization and coordinate directional movement.

Materials and methods

Materials

We obtained latrunculin A, LY294002, aprotinin, and leupeptin from Sigma-Aldrich, anti-myc antibodies from Santa Cruz Biotechnology, Inc., glutathione–Sepharose beads from GE Healthcare, and γ-[^{32}P]ATP from MP Biomedicals. Anti-Rap1 antibodies have been described previously (Kang et al., 2002). 13-mm nitrocellulose filters (0.22 μm) used for the adhesion assay were obtained from Millipore.

Strains and plasmids

The full coding sequence of the *rap1* cDNA was generated by RT-PCR and was subcloned into the EcoRI–XhoI site of pSP72. An EcoRI restriction site in the 5′ end region of the *rap1* gene was removed by substitution of cytosine at nucleotide 18 with thymine without changing the coding of amino acids. For GFP- or myc-Rap1 fusion proteins, the EcoRI–XhoI fragments of pSP72 were subcloned into the expression vector EXP-4(+) containing either a GFP or myc fragment.

The mutants $Rap1^{G12V}$ and $Rap1^{S17N}$ were generated using the QuikChange Site-Directed Mutagenesis kit (Stratagene). Because the *D. discoideum rap1* gene product contains two additional N-terminal amino acids compared with the human *rap1* and *ras* gene products, amino acids were numbered according to the consensus alignment of Ras proteins to facilitate comparison (Rebstein et al., 1997). GST-RalGDS–Ras-binding domain (RBD) was a gift from J.L. Bos (University Medical Center Utrecht, Utrecht, Netherlands). For RBD-RalGDS-YFP fusion protein expression, the RBD of RalGDS was amplified by PCR using GST-RB-RalGDS as a template, was ligated to a YFP fragment, and was cloned into the expression vector EXP-4(+). All clones were confirmed by DNA sequencing.

A *phg2* knockout construct was made by inserting the blasticidin resistance cassette into a BamHI site created at nucleotide 595 of the *phg2* cDNA and was used for a gene replacement in the KAx-3 parental strains. Randomly selected clones were screened for a gene disruption by PCR, which was then confirmed by Southern blot analysis and RT-PCR. These studies confirmed that the knockout strains did not express Phg2 transcripts 5′ or 3′ to the site of insertion.

A full-length *phg2* sequence was obtained by PCR using a series of primers and was cloned into pBluescript, sequenced, and subcloned into EXP-4(+) plasmids for GFP or GST fusion protein expression. To create a GFP-Phg2 construct lacking the RA domain (GFP-Phg2ΔRA), two pairs of primers were used to amplify the sequence 5′ and 3′ to that encoding the RA domain, creating an XbaI site at the junction site. This created an in-frame deletion of the RA domain. This construct was then subcloned into GFP-fused pEXP4 plasmid. The GFP-Phg2ΔRA coding region was confirmed by sequencing.

The *mhca*-null mutant strain in the KAx-3 background and MhcA-GFP plasmids were provided by J.A. Spudich (Stanford University, Palo Alto, CA). The *myosin VII*– and *talin A*–null cells were obtained from M.A. Titus (University of Minnesota, Minneapolis, MN), and DH1-10 and *phg2*-null cells in the DH1-10 background were obtained from P. Cosson (Universite de Geneve, Geneva, Switzerland). The myosin heavy chain phosphorylation mutant constructs 3XAsp and 3XAla were gifts from T.T. Egelhoff (Case Western Reserve University, Cleveland, OH).

Rap1 activation assay

The Rap1-GTP–binding domain of mammalian RalGDS was expressed in *E. coli* as a GST fusion protein as described previously (Franke et al., 1997). The purified GST-RalGDS-RBD was used for the detection of activated Rap1. Log-phase vegetative cells were washed twice and resuspended at a density of 5×10^6 cells/ml in Na/K phosphate buffer and pulsed for 6 h with 30 nM cAMP every 6 min. The cells were collected and resuspended at a density of 2×10^7 cells/ml and were treated with 1 mM caffeine for 30 min. The 300-μl aliquots were stimulated with

15 μM cAMP and lysed by mixing with an equal volume of 2× lysis buffer (100 mM Tris, pH 7.5, 300 mM NaCl, 50 mM $MgCl_2$, 20% glycerol, 1% NP-40, 2 mM DTT, 2 mM vandate, aprotinin, and 5 μg/ml leupeptin) at the indicated times. The lysates were centrifuged for 10 min, and the supernatants were incubated with 10 μg GST-RBD on glutathione–Sepharose beads at 4°C for 30 min in the presence of 1 mg/ml BSA. The beads were washed three times and subjected to SDS-PAGE and Western blot analysis with either an anti-myc mAb or an anti-Rap1 pAb. For control of the input amount of total Rap1 proteins, 40 μl of the cells were taken right after lysis of the cells and analyzed.

Chemotaxis and image acquisition

Analyses of chemotaxis toward cAMP were performed as described previously (Park et al., 2004; Sasaki et al., 2004). The images of chemotaxing cells were taken at time-lapse intervals of 6 s for 30 min using an inverted microscope (TE300; Nikon) with a plan Fluor ELWD 40× NA 0.6 lens and a camera (CoolSnap HQ; Roper Scientific). The frames were captured using MetaMorph software (Molecular Devices), and the data were analyzed using DIAS software (Soll Technologies; Wessels et al., 1998). Cells for analysis were randomly chosen with the requirement that they move for at least 15 min without touching another cell and were examined. Differential interference contrast images were hand traced (10 frames/min for 15–20 min). At least five randomly chosen cells were analyzed from each of at least three independent experiments performed on separate days.

The quantitation of membrane or cortical localization of GFP fusion proteins was performed as described previously (Sasaki et al., 2004) with slight modification. Fluorescence images were obtained using a confocal microscope (DM IRE2; Leica) with HCX plan Apo NA 1.40 100× or 63× objective lenses (oil CS; Leica) and a camera (EM-CCD or ORCA-ER; Hamamatsu Photonics). Images were captured using SimplePCI software (Compix Inc., Imaging Systems) and were analyzed using ImageJ software (National Institutes of Health). Differential interference contrast images were taken with the same equipment but using an ORCA-285 camera (Hamamatsu Photonics).

Cell attachment assay

Adhesion assays were performed as described previously (Sun et al., 2003) with minor modifications. Log-phase growing cells on the plates were washed with Na/K phosphate buffer and resuspended at a density of 2×10^6 cells/ml. The amount of 4×10^5 cells in 200 μl were plated onto 13-mm circular nitrocellulose filters (Millipore). After 30 min, unattached cells were removed by dipping filters into Na/K phosphate buffer. Filters were transferred to microcentrifuge tubes filled with 800 μl Na/K phosphate buffer and were vortexed for 1 min with a mixer (model 5432; Eppendorf) simultaneously. 150 μl of the detached cells from the filters were plated onto a 30-mm Petri plate with a hole covered by a 0.17-mm glass coverslip, and an additional coverslip was placed on top. The cells were photographed and counted (detached cell number). To determine the total cell number, 200 μl of the cells was transferred into microcentrifuge tubes filled with 600 μl Na/K phosphate buffer and counted. Cell adhesion is presented as a percentage of detached cells compared with total cells. This experiment was repeated three times or more, each time with four filters for each strain.

Cytoskeleton kinase activity assay

5×10^6 cells/ml in Na/K phosphate buffer were pulsed and stimulated with cAMP as described in the PKB/Akt activity assay (Meili et al., 1999). After stimulation with cAMP, the cells were lysed by mixing with an equal volume of 2× lysis buffer. The cytoskeleton fractions were isolated by centrifugation of the lysates at 4°C for 10 min. The pellets were washed once with 1× lysis buffer and then with kinase buffer (25 mM MOPS, pH 7.4, 25 mM β-glycerophosphate, 20 mM $MgCl_2$, and 1 mM DTT). The pellets were resuspended and incubated in 50 μl of kinase buffer containing 10 μCi γ-[^{32}P]ATP and 5 μM ATP for 20 min at 22°C. The reaction was stopped by the addition of 25 μl of 4× sample buffer followed by SDS-PAGE. The gels were stained with Coomassie blue, dried on a Hoefer slab gel drying apparatus, and exposed to film.

Biochemical assays

F-actin polymerization and myosin II assembly were assayed as described previously (Park et al., 2004). Fluid-phase endosomes were labeled using 70,000-M_r TRITC-dextran (Sigma-Aldrich). Log-phase cells expressing GFP-Rap1 proteins were incubated with 0.75 mg/ml TRITC-dextran for 1 h and were washed twice with Na/K phosphate buffer. The cells were observed using a confocal microscope (DM IRE2; Leica). Sodium azide treatment of cells was performed as described previously (Pasternak et al., 1989). Vegetative cells were washed twice with MES buffer (20 mM MES, pH 6.8, 2 mM $MgSO_4$, and 0.2 mM $CaCl_2$) and oxygenated by bubbling for 20 min. The cells were allowed to adhere to glass coverslips for 10 min and were inverted onto a plate with a hole covered by a glass coverslip holding 150 μl MES buffer with or without 25 μM NaN_3. After 30 min of incubation, the cells were photographed.

Online supplemental material

Fig. S1 shows that the *phg2*-null strain created in the KAx-3 background exhibits strong attachment both in the plate-shaking method described in Kortholt et al. (2006) and in the cell attachment assay described in Materials and methods. Fig. S2 shows an increased number of turns and more frequent extrusion of lateral pseudopodia in cells expressing $Rap1^{G12V}$. Fig. S3 shows that the multicellular development of $Rap1^{OE}$ and $Rap1^{G12V}$ cells is delayed. In contrast, $Rap1^{S17N}$ cells develop more rapidly than wild-type cells. Fig. S4 shows basal levels of F-actin and assembled myosin II in vegetative cells or in aggregation-competent cells. Online supplemental material is available at http://www.jcb.org/cgi/content/full/jcb.200607072/DC1.

We would like to thank Tom Egelhoff for his helpful suggestions and for providing *mhck-A/-B/-C*–null cells and *mhca*-null cells expressing 3XAla–myosin II. We also thank Peter van Haastert for stimulating discussions, Pierre Cosson for the *phg2*-null strain and discussions of his group's results, and Jim Spudich for the anti–myosin II antibody. We thank the other members of the Firtel laboratory for advice and assistance.

This work was supported by grants from the U.S. Public Health Service to R.A. Firtel and grants from the Canadian Institutes of Health Research to G. Weeks.

Submitted: 17 July 2006
Accepted: 9 February 2007

References

Arthur, W.T., L.A. Quilliam, and J.A. Cooper. 2004. Rap1 promotes cell spreading by localizing Rac guanine nucleotide exchange factors. *J. Cell Biol.* 167:111–122.

Asakura, T., H. Nakanishi, T. Sakisaka, K. Takahashi, K. Mandai, M. Nishimura, T. Sasaki, and Y. Takai. 1999. Similar and differential behaviour between the nectin-afadin-ponsin and cadherin-catenin systems during the formation and disruption of the polarized junctional alignment in epithelial cells. *Genes Cells*. 4:573–581.

Berger, G., R. Quarck, D. Tenza, S. Levy-Toledano, J. de Gunzburg, and E.M. Cramer. 1994. Ultrastructural localization of the small GTP-binding protein Rap1 in human platelets and megakaryocytes. *Br. J. Haematol.* 88:372–382.

Bivona, T., H. Wiener, I. Ahearn, J. Siletti, V. Chiu, and M. Philips. 2004. Rap1 up-regulation and activation on plasma membrane regulates T cell adhesion. *J. Cell Biol.* 164:461–470.

Blanc, C., S. Charette, N. Cherix, Y. Lefkir, P. Cosson, and F. Letourneur. 2005. A novel phosphatidylinositol 4,5-bisphosphate-binding domain targeting the Phg2 kinase to the membrane in *Dictyostelium* cells. *Eur. J. Cell Biol.* 84:951–960.

Bos, J.L. 2005. Linking Rap to cell adhesion. *Curr. Opin. Cell Biol.* 17:123–128.

Bos, J.L., K. de Bruyn, J. Enserink, B. Kuiperij, S. Rangarajan, H. Rehmann, J. Riedl, J. de Rooij, F. van Mansfeld, and F. Zwartkruis. 2003. The role of Rap1 in integrin-mediated cell adhesion. *Biochem. Soc. Trans.* 31:83–86.

Bosgraaf, L., and P.J. van Haastert. 2006. The regulation of myosin II in *Dictyostelium*. *Eur. J. Cell Biol.* 85:969–979.

Bosgraaf, L., H. Russcher, J.L. Smith, D. Wessels, D.R. Soll, and P.J. Van Haastert. 2002. A novel cGMP signalling pathway mediating myosin phosphorylation and chemotaxis in *Dictyostelium*. *EMBO J.* 21:4560–4570.

Bosgraaf, L., A. Waijer, R. Engel, A.J. Visser, D. Wessels, D. Soll, and P.J. van Haastert. 2005. RasGEF-containing proteins GbpC and GbpD have differential effects on cell polarity and chemotaxis in *Dictyostelium*. *J. Cell Sci.* 118:1899–1910.

Clow, P.A., and J.G. McNally. 1999. In vivo observations of myosin II dynamics support a role in rear retraction. *Mol. Biol. Cell*. 10:1309–1323.

De la Roche, M.A., J.L. Smith, V. Betapudi, T.T. Egelhoff, and G.P. Cote. 2002. Signaling pathways regulating *Dictyostelium* myosin II. *J. Muscle Res. Cell Motil.* 23:703–718.

Egelhoff, T.T., R.J. Lee, and J.A. Spudich. 1993. *Dictyostelium* myosin heavy chain phosphorylation sites regulate myosin filament assembly and localization in vivo. *Cell*. 75:363–371.

Egelhoff, T., D. Croft, and P. Steimle. 2005. Actin activation of myosin heavy chain kinase A in *Dictyostelium. J. Biol. Chem.* 280:2879–2887.

Enserink, J., L. Price, T. Methi, M. Mahic, A. Sonnenberg, J. Bos, and K. Tasken. 2004. The cAMP-Epac-Rap1 pathway regulates cell spreading and cell adhesion to laminin-5 through the alpha-3-beta-1 integrin but not the alpha-6-beta-4 integrin. *J. Biol. Chem.* 279:44889–44896.

Franke, B., J.W. Akkerman, and J.L. Bos. 1997. Rapid Ca2+-mediated activation of Rap1 in human platelets. *EMBO J.* 16:252–259.

Fujita, H., S. Fukuhara, A. Sakurai, A. Yamagishi, Y. Kamioka, Y. Nakaoka, M. Masuda, and N. Mochizuki. 2005. Local activation of Rap1 contributes to directional vascular endothelial cell migration accompanied by extension of microtubules on which RAPL, a Rap1-associating molecule, localizes. *J. Biol. Chem.* 280:5022–5031.

Fukuhra, S., A. Sakurai, A. Yamagishi, K. Sako, and N. Mochizuki. 2006. Vascular endothelial cadherin-mediated cell–cell adhesion regulated by a small GTPase, Rap1. *J. Biochem. Mol. Biol*. 39:132–139.

Fukuyama, T., H. Ogita, T. Kawakatsu, T. Fukuhara, T. Yamada, T. Sato, K. Shimizu, T. Nakamura, M. Matsuda, and Y. Takai. 2005. Involvement of the c-Src-Crk-C3G-Rap1 signaling in the nectin-induced activation of Cdc42 and formation of adherens junctions. *J. Biol. Chem.* 280:815–825.

Gebbie, L., M. Benghezal, S. Cornillon, R. Froquet, N. Cherix, M. Malbouyres, Y. Lefkir, C. Grangeasse, S. Fache, J. Dalous, et al. 2004. Phg2, a kinase involved in adhesion and focal site modeling in *Dictyostelium. Mol. Biol. Cell*. 15:3915–3925.

Hall, A., V. Warren, and J. Condeelis. 1989. Transduction of the chemotactic signal to the actin cytoskeleton of *Dictyostelium discoideum. Dev. Biol.* 136:517–525.

Herrmann, C., G. Horn, M. Spaargaren, and A. Wittinghofer. 1996. Differential interaction of the Ras family GTP-binding proteins H-Ras, Rap1A, and R-Ras with the putative effector molecules Raf kinase and Ral-guanine nucleotide exchange factor. *J. Biol. Chem.* 271:6794–6800.

Kang, R., H. Kae, H. Ip, G.B. Spiegelman, and G. Weeks. 2002. Evidence for a role for the *Dictyostelium* Rap1 in cell viability and the response to osmotic stress. *J. Cell Sci.* 115:3675–3682.

Kinashi, T., and K. Katagiri. 2005. Regulation of immune cell adhesion and migration by regulator of adhesion and cell polarization enriched in lymphoid tissues. *Immunology*. 116:164–171.

Kortholt, A., H. Rehmann, H. Kae, L. Bosgraaf, I. Keizer-Gunnink, G. Weeks, A. Wittinghofer, and P.J. Van Haastert. 2006. Characterization of the GbpD-activated Rap1 pathway regulating adhesion and cell polarity in *Dictyostelium discoideum*. *J. Biol. Chem.* 281:23367–23376.

Krause, M., J.D. Leslie, M. Stewart, E.M. Lafuente, F. Valderrama, R. Jagannathan, G.A. Strasser, D.A. Rubinson, H. Liu, M. Way, et al. 2004. Lamellipodin, an Ena/VASP ligand, is implicated in the regulation of lamellipodial dynamics. *Dev. Cell*. 7:571–583.

Krugmann, S., S. Andrews, L. Stephens, and P.T. Hawkins. 2006. ARAP3 is essential for formation of lamellipodia after growth factor stimulation. *J. Cell Sci.* 119:425–432.

Lafuente, E.M., A.A. van Puijenbroek, M. Krause, C.V. Carman, G.J. Freeman, A. Berezovskaya, E. Constantine, T.A. Springer, F.B. Gertler, and V.A. Boussiotis. 2004. RIAM, an Ena/VASP and profilin ligand, interacts with Rap1-GTP and mediates Rap1-induced adhesion. *Dev. Cell*. 7:585–595.

Lee, J.H., K.S. Cho, J. Lee, D. Kim, S.B. Lee, J. Yoo, G.H. Cha, and J. Chung. 2002. *Drosophila* PDZ-GEF, a guanine nucleotide exchange factor for Rap1 GTPase, reveals a novel upstream regulatory mechanism in the mitogen-activated protein kinase signaling pathway. *Mol. Cell. Biol.* 22:7658–7666.

Levi, S., M.V. Polyakov, and T.T. Egelhoff. 2002. Myosin II dynamics in *Dictyostelium*: determinants for filament assembly and translocation to the cell cortex during chemoattractant responses. *Cell Motil. Cytoskeleton*. 53:177–188.

Liu, G., and P.C. Newell. 1991. Evidence that cyclic GMP may regulate the association of myosin-II heavy chain with the cytoskeleton by inhibiting its phosphorylation. *J. Cell Sci.* 98:483–490.

Meili, R., C. Ellsworth, S. Lee, T.B.K. Reddy, H. Ma, and R.A. Firtel. 1999. Chemoattractant-mediated transient activation and membrane localization of Akt/PKB is required for efficient chemotaxis to cAMP in *Dictyostelium. EMBO J.* 18:2092–2105.

Niewohner, J., I. Weber, M. Maniak, A. Muller-Taubenberger, and G. Gerisch. 1997. Talin-null cells of *Dictyostelium* are strongly defective in adhesion to particle and substrate surfaces and slightly impaired in cytokinesis. *J. Cell Biol.* 138:349–361.

Ohba, Y., K. Kurokawa, and M. Matsuda. 2003. Mechanism of the spatio-temporal regulation of Ras and Rap1. *EMBO J.* 22:859–869.

Pagh, K., H. Maruta, M. Claviez, and G. Gerisch. 1984. Localization of two phosphorylation sites adjacent to a region important for polymerization on the tail of *Dictyostelium* myosin. *EMBO J.* 3:3271–3278.

Park, K.C., F. Rivero, R. Meili, S. Lee, F. Apone, and R.A. Firtel. 2004. Rac regulation of chemotaxis and morphogenesis in *Dictyostelium. EMBO J.* 23:4177–4189.

Pasternak, C., J.A. Spudich, and E.L. Elson. 1989. Capping of surface receptors and concomitant cortical tension are generated by conventional myosin. *Nature*. 341:549–551.

Rebhun, J.F., A.F. Castro, and L.A. Quilliam. 2000. Identification of guanine nucleotide exchange factors (GEFs) for the Rap1 GTPase. Regulation of MR-GEF by M-Ras-GTP interaction. *J. Biol. Chem.* 275:34901–34908.

Rebstein, P.J., G. Weeks, and G.B. Spiegelman. 1993. Altered morphology of vegetative amoebae induced by increased expression of the *Dictyostelium discoideum* ras-related gene rap1. *Dev. Genet.* 14:347–355.

Rebstein, P.J., J. Cardelli, G. Weeks, and G.B. Spiegelman. 1997. Mutational analysis of the role of Rap1 in regulating cytoskeletal function in *Dictyostelium. Exp. Cell Res.* 231:276–283.

Retta, S.F., F. Balzac, and M. Avolio. 2006. Rap1: a turnabout for the crosstalk between cadherins and integrins. *Eur. J. Cell Biol.* 85:283–293.

Sasaki, A.T., and R.A. Firtel. 2006. Regulation of chemotaxis by the orchestrated activation of Ras, PI3K, and TOR. *Eur. J. Cell Biol.* 85:873–895.

Sasaki, A.T., C. Chun, K. Takeda, and R.A. Firtel. 2004. Localized Ras signaling at the leading edge regulates PI3K, cell polarity, and directional cell movement. *J. Cell Biol.* 167:505–518.

Steimle, P.A., S. Yumura, G.P. Cote, Q.G. Medley, M.V. Polyakov, B. Leppert, and T.T. Egelhoff. 2001. Recruitment of a myosin heavy chain kinase to actin-rich protrusions in *Dictyostelium. Curr. Biol.* 11:708–713.

Stork, P.J. 2003. Does Rap1 deserve a bad Rap? *Trends Biochem. Sci.* 28:267–275.

Sun, B., H. Ma, and R.A. Firtel. 2003. *Dictyostelium* stress-activated protein kinase alpha, a novel stress-activated mitogen-activated protein kinase kinase kinase-like kinase, is important for the proper regulation of the cytoskeleton. *Mol. Biol. Cell*. 14:4526–4540.

Tuxworth, R.I., S. Stephens, Z.C. Ryan, and M.A. Titus. 2005. Identification of a myosin VII-Talin complex. *J. Biol. Chem.* 280:26557–26564.

Van Haastert, P.J., and P.N. Devreotes. 2004. Chemotaxis: signalling the way forward. *Nat. Rev. Mol. Cell Biol.* 5:626–634.

Weeks, G., P. Gaudet, and R.H. Insall. 2005. The small GTPase superfamily. *In Dictyostelium* Genomics. W.F. Loomis and A. Kuspa, editors. Horizon Bioscience, Norfold, UK. 211–234.

Wessels, D., E. Voss, N. Von Bergen, R. Burns, J. Stites, and D.R. Soll. 1998. A computer-assisted system for reconstructing and interpreting the dynamic three-dimensional relationships of the outer surface, nucleus and pseudopods of crawling cells. *Cell Motil. Cytoskeleton*. 41:225–246.

Wong, K., O. Pertz, K. Hahn, and H. Bourne. 2006. Neutrophil polarization: spatiotemporal dynamics of RhoA activity support a self-organizing mechanism. *Proc. Natl. Acad. Sci. USA*. 103:3639–3644.

Yumura, S., and T. Kitanishi-Yumura. 1992. Release of myosin II from the membrane-cytoskeleton of *Dictyostelium discoideum* mediated by heavy-chain phosphorylation at the foci within the cortical actin network. *J. Cell. Biol*. 117:1231–1239.

Yumura, S., M. Yoshida, V. Betapudi, L.S. Licate, Y. Iwadate, A. Nagasaki, T.Q. Uyeda, and T.T. Egelhoff. 2005. Multiple myosin II heavy chain kinases: roles in filament assembly control and proper cytokinesis in *Dictyostelium. Mol. Biol. Cell*. 16:4256–4266.